Journal of Hazardous Materials 339 (2017) 264–273

Contents lists available at ScienceDirect

Journal of Hazardous Materials

journal homepage: www.elsevier.com/locate/jhazmat

Influence of natural organic matter (NOM) coatings on nanoparticle adsorption onto supported lipid bilayers

Zhang Bo[d], Saziye Yorulmaz Avsar[a,b,c], Michael K. Corliss[a,b,c], Minsub Chung[e], Nam-Joon Cho[a,b,c,*]

[a] School of Materials Science and Engineering, Nanyang Technological University, 50 Nanyang Avenue 639798, Singapore
[b] Centre for Biomimetic Sensor Science, Nanyang Technological University, 50 Nanyang Drive, 637553, Singapore
[c] School of Chemical and Biomedical Engineering, Nanyang Technological University, 62 Nanyang Drive 637459, Singapore
[d] Shanghai Jiao Tong University Environment Science Building, 800 Dongchuan Rd, Minhang District, Shanghai 200240, China
[e] Department of Chemical Engineering, Hongik University, Mapo-gu, Seoul 04066, Republic of Korea

HIGHLIGHTS

- Interaction of Ag and C_{60} nanoparticles with charged lipid membranes was studied.
- Quartz crystal microbalance experiments measured the adsorption kinetics.
- Natural organic matter (NOM) either inhibited or promoted nanoparticle adsorption.
- Adsorption profile depended on nanoparticle type, electrolyte condition, and NOM.

ARTICLE INFO

Article history:
Received 16 February 2017
Received in revised form 31 May 2017
Accepted 15 June 2017
Available online 21 June 2017

Keywords:
Supported lipid bilayer
Quartz crystal microbalance-dissipation
Nanoparticle
Natural organic matter
Nanoparticle-membrane interaction

ABSTRACT

As the worldwide usage of nanoparticles in commercial products continues to increase, there is growing concern about the environmental risks that nanoparticles pose to biological systems, including potential damage to cellular membranes. A detailed understanding of how different types of nanoparticles behave in environmentally relevant conditions is imperative for predicting and mitigating potential membrane-associated toxicities. Herein, we investigated the adsorption of two popular nanoparticles (silver and buckminsterfullerene) onto biomimetic supported lipid bilayers of varying membrane charge (positive and negative). The quartz crystal microbalance-dissipation (QCM-D) measurement technique was employed to track the adsorption kinetics. Particular attention was focused on understanding how natural organic matter (NOM) coatings affect nanoparticle-bilayer interactions. Both types of nanoparticles preferentially adsorbed onto the positively charged bilayers, although NOM coatings on the nanoparticle and lipid bilayer surfaces could either inhibit or promote adsorption in certain electrolyte conditions. While past findings showed that NOM coatings inhibit membrane adhesion, our findings demonstrate that the effects of NOM coatings are more nuanced depending on the type of nanoparticle and electrolyte condition. Taken together, the results demonstrate that NOM coatings can modulate the lipid membrane interactions of various nanoparticles, suggesting a possible way to improve the environmental safety of nanoparticles.

1. Introduction

Ongoing advances in nanoscience and nanotechnology have heralded a new age of innovation across a wide range of fields, including food science, environmental remediation, cosmetics, textiles, paints, and pharmaceuticals [1]. Subsequently, these advances have led to a significant increase in the usage of nanotechnology-inspired products (*e.g.*, batteries [2], face creams [3], food storage bins [4] and bandages [5]) based on engineered nanoparticles (NPs). Among different types of NPs, silver nanoparticles (AgNPs) and derivatives of water-stable fullerene nanoparticle aggregates (C_{60}NPs) have been widely investigated as models for inorganic and organic, carbon-based nanomaterials, respectively. AgNPs are found in many commercial products and have demonstrated toxic-

* Corresponding author at: School of Materials Science and Engineering, Nanyang Technological University, 50 Nanyang Avenue 639798, Singapore.
E-mail address: njcho@ntu.edu.sg (N.-J. Cho).

http://dx.doi.org/10.1016/j.jhazmat.2017.06.031
0304-3894/

ities against numerous organisms and cell lines, inspiring extensive research into the environmental impact of AgNPs and transformation products in the environment [6,7]. Likewise, C_{60}NPs have low toxicity but can remain in soil and other deposits for extended periods due to poor bioavailability [8]. To date, the majority of related studies have focused on human health implications of nanoparticles, although recent literature has also increasingly focused on the ecological implications of nanoparticles with respect to their fate and toxicity [9–11]. The interaction of nanoparticles with environmental systems has been principally studied with respect to bioaccumulation and biotoxicity [12–22]. Understanding how the physicochemical properties of nanoparticles and their surface functionalization influences these activities is a key objective.

The interactions between nanoparticles and cell membranes largely determine the degree of toxicity for a particular class of nanoparticle. When nanoparticles interact with a cell membrane, they can adsorb onto the membrane surface and, in some cases, penetrate the membrane, resulting in cellular uptake and/or membrane damage [23–26]. To systematically characterize the interactions between nanoparticles and cell membranes, various kinds of biomimetic cell membrane platforms have been experimentally utilized, including lipid vesicle suspensions [27], black lipid membranes [28], mercury droplet membranes [29], giant unilamellar vesicles [30], tethered lipid bilayers, and supported lipid bilayers (SLBs) [31]. Due to their versatility, SLB platforms are one of the most commonly used model membranes for characterizing the interactions of molecules with cell membranes [32], and have been utilized to mimic human and bacterial cell membranes [33,34]. Indeed, SLB platforms of different lipid compositions can be fabricated on hydrophilic substrates by utilizing the solvent-assisted lipid bilayer (SALB) formation method [35,36] and a wide range of surface-sensitive measurement techniques such as the quartz crystal microbalance-dissipation (QCM-D), atomic force microscopy (AFM), and electrochemical impedance spectroscopy (EIS), can be used to monitor SLB formation and nanoparticle-membrane interactions [37]. Previous studies showed that nanoparticles can adsorb onto SLBs and either simply adsorb without damage or cause different types of membrane disruption such as pore formation and lipid solubilization depending on the system [38–40]. So far, the corresponding measurements have been typically conducted in pristine conditions and extending such measurements to include additional environmental factors would improve our knowledge about how nanoparticle-membrane interactions might occur in the environment.

Nanoparticles can undergo physical and chemical transformations depending on environmental conditions such as sunlight and temperature [41], as well as due to interactions with natural organic matter (NOM) that is ubiquitous in aquatic environments [42–45]. To study how environmental factors affect solution-phase nanoparticles, simplified experimental conditions that mimic aquatic environmental conditions have been utilized based on modulating NOM and electrolyte components. In general, it is understood that higher ionic strength conditions cause nanoparticle aggregation that further depends on the ion species [46,47]. Moreover, NOM is a particularly important determinant of nanoparticle fate in environmental systems. As the byproduct of decomposed organisms, NOM contains a diversity of hydrophobic lipids and proteins in addition to high molecular weight humic and fulvic acids, and the resulting mixture of molecular compounds contains a wide range of hydroxyl, alcohol, carbonyl, methoxy, carboxylic and phenolic functional groups [48–50]. As a result, NOM can easily coat nanoparticle surfaces [47–51] and replace weakly bound coating agents (*e.g.*, noncovalently attached surfactants) to form heterogeneous molecular coating layers [50]. To our knowledge, there is no previous report detailing the effects of NOM on the interaction between nanoparticles and cell membranes.

In this study, we have systematically investigated the interaction of two well-studied nanoparticles, AgNPs and C_{60}NPs, with SLB platforms in the presence and absence of NOM and in different monovalent and divalent electrolyte solutions (NaCl or $CaCl_2$). SLBs were fabricated with either positive or negative surface charges by using the SALB fabrication method. The QCM-D measurement technique was utilized to monitor the kinetics of nanoparticle-membrane interactions in a label-free format that does not require chemical labeling of either the SLB or nanoparticles [51,52]. Furthermore, we employed two different experimental scenarios to monitor the membrane-NP interactions in the presence of NOM, as outlined in Fig. 1. In the first scenario, the SLB was initially coated with NOM and then NPs were injected in order to mimic the situation when pristine NPs are first introduced into the environment. In the second scenario, NOM and NPs were initially mixed and subsequently added to the SLB platform, thereby more closely mimicking situations where both the cellular membranes and NPs have been present in the environment for some time.

2. Materials and methods

2.1. Materials

1,2-dioleoyl-*sn*-glycero-3-phosphocholine (DOPC), 1,2-dioleoyl-*sn*-glycero-3-ethylphosphocholine (chloride salt) (DOEPC), and 1-palmitoyl-2-oleoyl-*sn*-glycero-3-phospho-(1′-*rac*-glycerol) (sodium salt) (POPG) were obtained in lyophilized powder form from Avanti Polar Lipids (Alabaster, AL). The lipid powders were stored at −20 °C and dissolved in appropriate organic solvents immediately prior to SALB bilayer formation experiments. Bovine serum albumin (BSA) was obtained from Sigma-Aldrich (St. Louis, MO). Two different nanoparticles (NPs) were used in the experiments: polyvinylpyrrolidone (PVP)-coated $AgNO_3$ (>99.5%) NPs were purchased from Shanghai Huzheng Nano Technology Co., Ltd (Shanghai, China) and fullerene (C_{60}) NPs (99.9% purified through sublimation) were obtained from the MER Corporation (Tucson, AZ). The PVP-coated $AgNO_3$ NPs (denoted as AgNPs) are a stabilized form that is recommended for situations where chronic exposure is anticipated [53]. Suwannee River Natural Organic Matter (SRNOM; defined as NOM in this work) (RO isolation, 2R101N) was received from the International Humic Substance Society (St. Paul, MN). All solutions were prepared with Milli-Q-treated water (>18 MΩ cm) (Millipore, Billerica, MA).

2.2. Preparation and characterization of nC_{60} aggregates and AgNPs

To emulate the fate of fullerenes upon release into the environment, water-soluble C_{60} aggregates (denoted as nC_{60}NPs) were prepared by stirring C_{60}NPs in ultrapure water for six months in dark storage, as previously described [54]. Dynamic light scattering (DLS) was used to measure the size distributions of nanoparticle samples based on the diffusion properties of the nanoparticles in solution. A 90Plus particle size analyzer (Brookhaven Instruments, Holtsville, NY) with a 658.0 nm monochromatic laser was employed for all measurements, which were taken at the fixed scattering angle of 90°. The intensity autocorrelation function was determined in order to calculate the intensity-weighted size distribution of nanoparticles. The size distributions of nanoparticles were reported based on the average effective hydrodynamic diameter and polydispersity in water, as well as in 10 mM NaCl or $CaCl_2$ aqueous solutions that contained varying concentrations of NOM (0–10 ppm). In natural freshwaters, NaCl or $CaCl_2$ are the most prevalent monovalent and divalent salts and hence were chosen as the electrolyte conditions for this study [55]. In physiological envi-

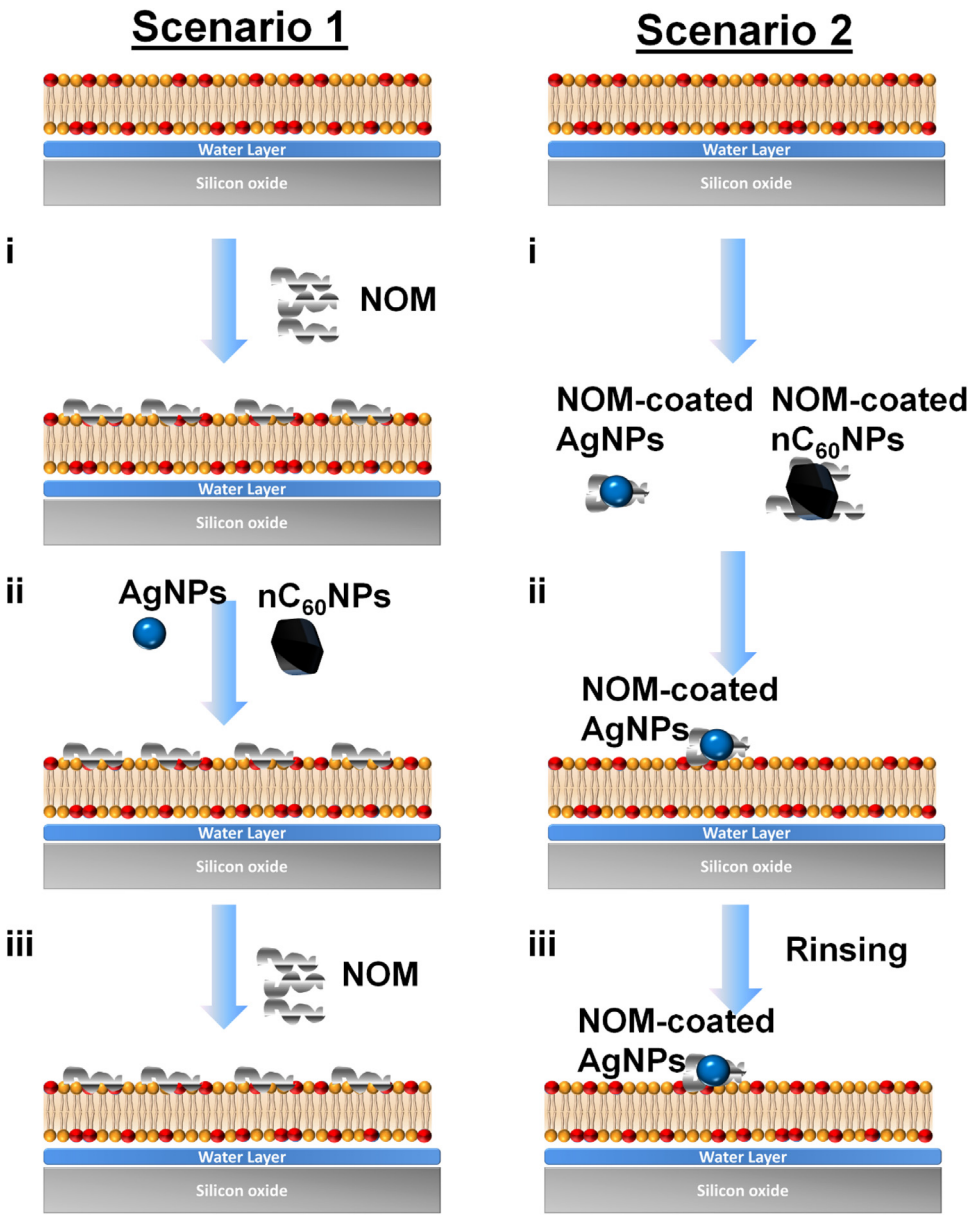

Fig. 1. Schematic illustration of experimental scenarios to investigate how NOM influences membrane-nanoparticle interactions. Scenario 1: Precoating of SLB platform with NOM components to mimic an environmentally relevant situation. Scenario 2: Preincubation of nanoparticles with NOM components, prior to adding nanoparticles + NOM to the SLB platform.

ronments, the Ca^{2+} concentration is typically 5 mM or lower and we chose a moderately higher concentration for direct comparison with monovalent salt conditions, as done in past studies [55] and in the range of tested concentrations [56,57]. To be in the optimal concentration range for DLS measurements, the tested nanoparticle concentrations were 1:10 dilutions of the stock solutions (0.25 ppm AgNPs or 45 nM nC_{60}NPs), and prepared samples were incubated for 30 min before experiment. Electrophoretic mobility measurements were conducted using a Delsa Nano C particle analyzer (Beckman Coulter, Brea, CA) in order to determine the zeta potential of nanoparticle suspensions. Each sample was measured 10 times for determining the zeta potential value (mean ± standard deviation). The experimental temperature was maintained at 25 °C for all measurements.

2.3. Quartz crystal microbalance-dissipation (QCM-D)

All QCM-D experiments were performed with a Q-Sense E4 instrument (Biolin Scientific AB, Gothenburg, Sweden) to monitor the interaction between nanoparticles (AgNPs and nC_{60}NPs) and an SLB platform in the presence and absence of NOM at varying concentrations. The QCM-D technique records changes in the resonance frequency (Δf) and energy dissipation (ΔD) of an oscillating silica-coated quartz crystal sensor chip (model no. QSX303) as a function of time, which reflect the acoustic mass and viscoelastic properties of an adsorbate on the sensor surface, respectively. In the present experiments, the SLB platform is coated on the QCM-D sensor surface such that nanoparticle adsorption onto the SLB can be measured by tracking the frequency shift. Specifically, the QCM-D technique enables measurement of the nanoparticle uptake

(amount of adsorbed mass) and the kinetics of the adsorption process.

Before experiment, the sensor chips were sequentially cleaned with 2% SDS, water and ethanol, dried with nitrogen gas, and then subjected to oxygen plasma treatment for 2 min with an Expanded Plasma Cleaner (model no.PDC-002, Harrick Plasma, Ithaca, NY). Two SLB platforms with different membrane surface charges were created by using the SALB fabrication procedure. DOPC (zwitterionic) and DOEPC (cationic) lipid powders were dissolved in isopropanol at a final concentration of 10 mg/mL. POPG (anionic) lipid powder was dissolved in ethanol at a final concentration of 5 mg/mL and incubated at 40 °C in order to aid lipid solubilization. Lipid solutions were mixed to a ratio of 70 mol% DOPC and 30 mol% DOEPC for preparation of positively charged SLB platforms and 70 mol% DOPC and 30 mol% POPG for preparation of negatively charged SLB platforms, and then diluted with isopropanol to a final concentration of 0.5 mg/mL.

As part of the SALB experimental procedure, a measurement baseline was first recorded in aqueous buffer solution (10 mM Tris [pH 7.5] with 150 mM NaCl), followed by exchange with isopropanol solution. Then, 0.5 mg/mL lipid in isopropanol was deposited onto the silicon oxide-coated substrate and allowed to equilibrate for approximately 10 min, followed by exchange with aqueous buffer solution that completed the SLB fabrication process. Next, 0.1 mg/mL BSA was added in order to estimate the fraction of SLB surface coverage as well as to passivate any exposed regions on the silica sensor surface and therefore concentrate on probing lipid membrane interactions. After the SLB formation procedure was completed, the running buffer solution was exchanged with distilled water supplemented with either 10 mM NaCl or 10 mM $CaCl_2$, and then the nanoparticles or NOM in the appropriate aqueous solution were injected. All QCM-D measurements were conducted under continuous flow conditions, with the flow rate chosen as 100 μL/min for all steps in the bilayer formation and washing processes and 41.8 μL/min for nanoparticles or NOM addition as controlled by a Reglo Digital peristaltic pump (Ismatec, Glattbrugg, Switzerland). During the experiments, the temperature in the measurement cell was maintained at 25.0 ± 0.5 °C. The QCM-D measurement data were collected at the 3rd, 5th, 7th, 9th, and 11th odd overtones, and the reported QCM-D data were obtained at the 5th overtone and normalized ($\Delta f_{n=5}/5$). Data processing was performed in the QTools (Q-Sense AB) and OriginPro 8.5 (OriginLab, Northampton, MA) software packages. Where applicable, the measurements were conducted in triplicate and reported as the mean ± standard deviation (s.d.).

3. Results and discussion

3.1. Morphological and zeta potential characterization of nanoparticles

We first characterized the effect of NOM on the size distribution of the NOM-treated nanoparticles in aqueous 10 mM NaCl or 10 mM $CaCl_2$ salt conditions, as presented in Figs. S1–S6. The intensity-weighted average hydrodynamic diameters of AgNPs alone were 62.6 nm in water, 74.3 nm in NaCl solution, and 111.9 nm in $CaCl_2$ solution. The presence of NOM in NaCl solution slightly increased the intensity-weighted average hydrodynamic diameters, confirming AgNP aggregation and the ability of NOM to inhibit aggregation. Higher concentrations of NOM decreased the intensity-weighted average hydrodynamic diameters of AgNPs from 94.4 nm (2.5 ppm) to 78.6 nm (10 ppm). In $CaCl_2$-containing solutions, increasing concentrations of NOM led to a decrease in the intensity-weighted average hydrodynamic diameters of AgNPs from 111.9 nm (0 ppm) down to 77.8 nm (2.5 ppm) and 53.6 nm (10 ppm). While NOM had a moderate effect on inhibiting AgNP aggregation in NaCl solutions, the effect was more pronounced in $CaCl_2$ solutions wherein significant reductions in AgNP aggregation were observed.

On the other hand, the intensity-weighted average hydrodynamic diameters for nC_{60}NPs were 336.1 nm in water, 310.6 nm in NaCl solution, and 850.1 nm in $CaCl_2$ solution. A high degree of aggregation is expected for nC_{60}NPs produced by extensive stirring in $CaCl_2$-containing water, hence confirming past findings [58]. In NaCl solution, the presence of NOM slightly decreased the intensity-weighted average hydrodynamic diameters from 310.6 nm (0 ppm) to 282.0 nm (2.5 ppm) and 237.3 nm (10 ppm). This finding is supported by previous observations that adsorption of NOM onto nC_{60}NPs stabilized nC_{60}NPs by promoting steric hindrance between nanoparticles [59,60]. As such, NOM was observed to promote disaggregation of nC_{60}NPs in a concentration-dependent manner as indicated by the decrease in particle size with increasing NOM concentration. Similar concentration-dependent disaggregation of nC_{60}NPs was also observed in $CaCl_2$ solutions, as increasing concentrations of NOM led to decreasing intensity-weighted average hydrodynamic diameters from 850.1 nm (0 ppm) to 806.4 nm (2.5 ppm) and 603.7 nm (10 ppm).

As evidenced by the data above, both types of nanoparticles aggregated in the presence of NaCl and $CaCl_2$ media, indicating that both monovalent and divalent electrolytes promote the aggregation of nanoparticles. In the case of monovalent electrolytes, this is most likely due to the screening of the electrostatic double-layer that reduces electrostatic repulsion between nanoparticles. Similar effects are also observed with divalent electrolytes and the divalent cations in particular likely also promote aggregation through more specific interactions with anionic functional groups. Following this line, the data further show that NOM can disaggregate AgNPs and nC_{60}NPs and reduce their size in NaCl and $CaCl_2$ media, as reported in previous studies [58–63]. In the case of nC_{60}NPs, NOM binding likely occurs to aromatic groups on the NP surface [64]. Hence, NOM appears to influence the surface properties of the two types of nanoparticles.

To further characterize the two nanoparticle systems, the pH-dependent zeta potential values of the AgNPs and nC_{60}NPs in the absence and presence of NOM were measured, as reported in Fig. S7. The data indicate that the surfaces of AgNPs and C_{60}NPs are negatively charged, and the latter's surface is more negatively-charged than the former. With increasing pH, the zeta potential values of nC_{60}NPs tended to become more negative down to approximately −43 mV, while the zeta potential values of AgNPs remained similar at around −15 mV across all tested pH conditions. Interestingly, the effect of NOM on the zeta potential values of AgNPs and nC_{60}NPs was quite distinct. For nC_{60}NPs, the NOM coating had negligible effect on the zeta potential values recorded at the different pH conditions. By contrast, the NOM coating increased the negative zeta potential values for AgNPs down to around −30 mV at the different pH conditions. As such, our initial characterization experiments identify that both the size and zeta potential values of the anionic AgNPs and nC_{60}NPs depend on the presence of NOM in the different electrolyte conditions and establish trends for interpreting the QCM-D measurement data.

3.2. Characterization of SLB platform for membrane-nanoparticle investigations

In order to monitor the adsorption kinetics of AgNPs and nC_{60}NPs onto lipid membranes, SLB platforms with different surface charges were first fabricated on silicon oxide substrates by using the SALB technique. Mixtures of 70 mol% DOPC and 30 mol% DOEPC were used to prepare positively charged SLBs, and mixtures of 70 mol% DOPC and 30 mol% anionic POPG were used to prepare negatively charged SLBs. The QCM-D technique was utilized

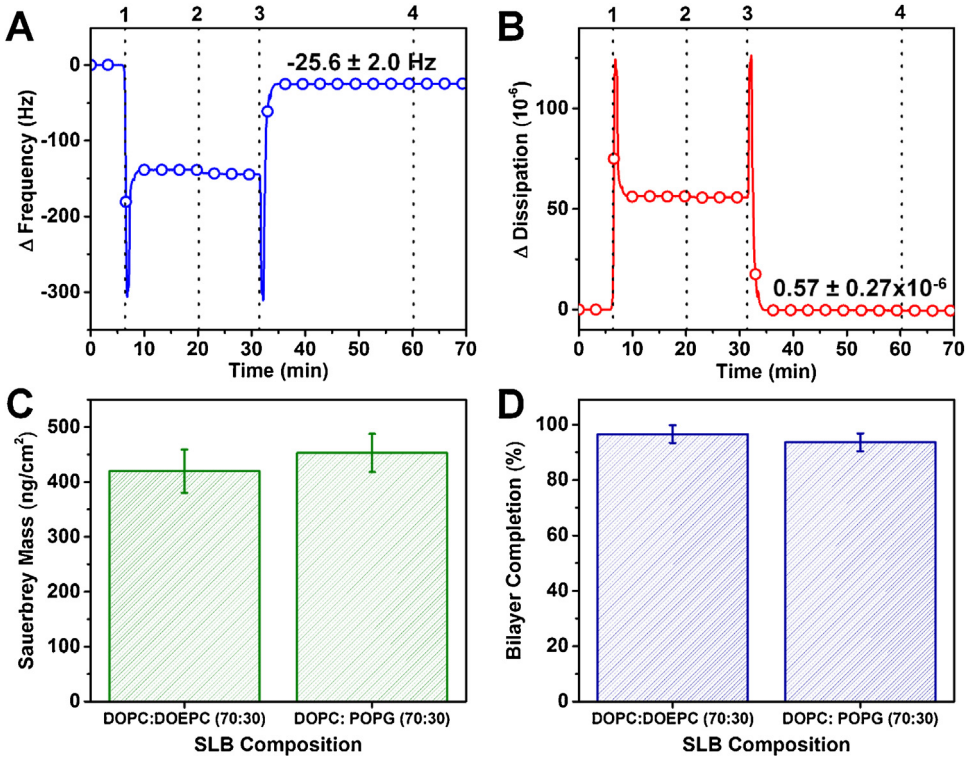

Fig. 2. Characterization of SLB formation process. QCM-D measurement of (A) resonance frequency and (B) energy dissipation shifts during SLB formation process. Baseline was recorded in aqueous buffer. Step 1: Inject isopropanol solution. Step 2: Add 0.5 mg/mL lipids in isopropanol. Step 3: Exchange isopropanol to aqueous buffer. Step 4: Add 0.1 mg/mL BSA protein. (C) Surface mass density of SLB platform based on Sauerbrey relationship. (D) Surface coverage of SLB platform based on protein binding capacity relative to a bare silica surface.

in order to characterize the SLB formation processes. Representative QCM-D sensorgrams of the resonance frequency and energy dissipation signals during the SLB formation process are shown in Fig. 2A,B. The measurement baselines were initially recorded in aqueous buffer solution (10 mM Tris, 150 mM NaCl, pH 7.5). After establishing stable measurement signals, isopropanol solution was injected into the measurement cell (Step 1) which led to significant changes in the frequency and energy dissipation due to differences in the bulk density and viscosity of the aqueous buffer *versus* isopropanol. Then, a freshly prepared 0.5 mg/mL lipid solution composed of either DOPC:DOEPC 70:30 dissolved in isopropanol or DOPC:POPG 70:30 dissolved in isopropanol was injected (Step 2). At the final step of the SALB method, the running isopropanol solution was gradually exchanged with buffer solution (Step 3), resulting in either a negatively or positively charged SLB platform with final frequency and energy dissipation shifts of -25.6 ± 2.0 Hz and $0.6 \pm 0.3 \times 10^{-6}$, respectively, which are in good agreement with earlier reported values [65–67] indicating successful SLB formation. By applying the Sauerbrey equation that relates the change in resonance frequency to adsorbed mass, the calculated mass of the SLBs was found to range between 400 and 450 ng/cm^2, which is consistent with SLB formation (Fig. 2C). Moreover, to estimate the surface coverage of the SLB coating on the sensor surface, nonspecific BSA adsorption onto bare and SLB-coated silicon oxides was measured and indicated that the SLBs had greater than 90% surface coverage (Fig. 2D).

3.3. *Effect of membrane surface charge on nanoparticle adsorption*

Using the SLB platform, the adsorption kinetics of AgNPs and nC_{60}NPs onto positively and negatively charged membranes were investigated. After SLB formation was completed, the running buffer was exchanged with a distilled water solution supplemented with 10 mM NaCl or 10 mM $CaCl_2$ and the QCM-D measurement responses were normalized to zero and then either 2.5 ppm AgNPs or 450 nM nC_{60}NPs were added in the presence of NaCl or $CaCl_2$ depending on the experiment. There was a general decrease in frequency shifts associated with the adsorption of nanoparticles onto the positively charged SLBs, indicating nanoparticle adsorption (Fig. 3A,B). There was significantly more adsorption of AgNPs onto positively charged SLBs in the presence of $CaCl_2$, as indicated by larger final frequency shifts (-17.9 ± 0.5 Hz) compared to the final frequency shifts in the presence of NaCl (-6.0 ± 0.3 Hz). By contrast, the adsorption of nC_{60}NPs onto positively charged SLB platforms was largely independent of the presence of NaCl or $CaCl_2$, with values around -18 Hz in both cases. These findings are consistent with nC_{60}NP attachment on the surface of the SLB platform [68,69]. In addition, the adsorption kinetics of nC_{60}NPs onto positively charged bilayers were appreciably slower than those of AgNPs. For example, adsorption of nC_{60}NPs reached equilibrium within 40 min while AgNPs reached equilibrium in less than 20 min. Considering that nanoparticle adsorption is diffusion-limited, this difference is likely due to the smaller size of the AgNPs which facilitates greater bulk diffusion (larger diffusion coefficient) and hence quicker adsorption uptake. A direct comparison of the absolute frequency shifts for AgNP and nC_{60}NP adsorption equilibrium is presented according to the different NP type and electrolyte composition (Fig. 3C). Similar absolute frequency shifts were obtained due to adsorption of both AgNPs and nC_{60}NPs in the presence of $CaCl_2$. By contrast, the absolute frequency shifts for nC_{60}NP adsorption were higher than those of AgNPs in the presence of NaCl. Furthermore, it was observed that both types of nanoparticles had minimal adsorption onto negatively charged bilayers in the presence of NaCl or $CaCl_2$, indicating that membrane association is likely mediated by attractive electrostatic forces (Fig. 3D,E). Hence, as

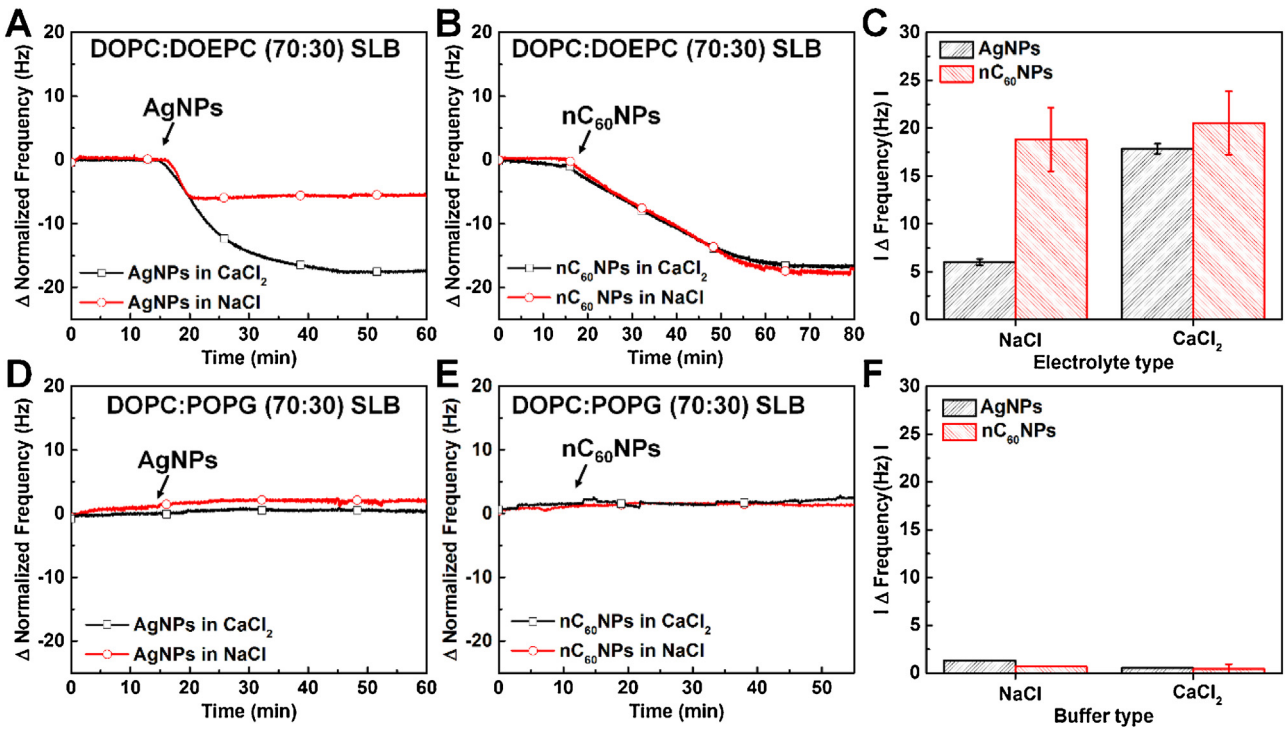

Fig. 3. Adsorption of AgNPs and nC_{60}NPs onto bare SLB platforms. QCM-D measurements track resonance frequency shifts, and 2.5 ppm AgNPs or 450 nM nC_{60}NPs were added to the SLB platform (see arrow). The solution conditions were 10 mM NaCl or $CaCl_2$. Addition of (A) AgNPs or (B) nC_{60}NPs onto positively charged SLBs. (C) Summary of absolute frequency shifts for NP adsorption data obtained in panels A–B. Addition of (D) AgNPs or (E) nC_{60}NPs onto negatively charged SLBs. (F) Summary of absolute frequency shifts for NP adsorption data obtained in panels D-E.

summarized in Fig. 3F, there were no effects of NaCl *versus* $CaCl_2$ on the absolute frequency shifts for nanoparticle adsorption onto negatively charged SLBs.

3.4. Effect of NOM-coated SLBs on nanoparticle adsorption

Fig. 4 presents the QCM-D measurement data for AgNP and nC_{60}NP adsorption onto NOM-coated, positively charged SLBs, as outlined in Scenario 1. The SLB platforms were first coated with different concentrations of NOM, and then the nanoparticles were added to the NOM-coated SLBs. In NaCl conditions, NOM adsorbed onto the positively charged SLBs largely independent of NOM concentration, with absolute frequency shifts around -5.1 ± 1.3 Hz (Fig. 4A,B). Interestingly, the presence of NOM coatings on the positively charged SLB platforms prevented subsequent adsorption of both AgNPs and nC_{60}NPs. There was no further change in the measurement responses when NOM was reintroduced into the system. On the other hand, when NOM was added in the presence of $CaCl_2$, the frequency shifts depended on the NOM concentration (Fig. 4C,D). For 2.5 ppm NOM concentration, there was a final frequency shift around -5.3 ± 5.0 Hz, whereas the frequency shift increased to around -14.3 ± 7.0 Hz at 10 ppm NOM concentration. As in the NaCl case, the NOM coating inhibited AgNP adsorption although to a lesser extent. Indeed, while AgNP adsorption in the absence of NOM yielded frequency shifts around -18 Hz, AgNP adsorption was significantly reduced by almost 73% on NOM-coated SLBs, with frequency shifts around -5 Hz (Fig. 4C). By contrast, NOM-coated SLBs appeared to inhibit nC_{60}NP adsorption in the presence of $CaCl_2$. In this particular case, positive frequency shifts were observed, indicating that nC_{60}NPs interacted with NOM components and removed them from the SLB surface (Fig. 4D). Subsequent addition of NOM led to negative frequency shifts that support nC_{60}NPs removed some of the SLB-attached NOM components in the preceding step. Collectively, the data support that NOM adsorbs onto positively charged SLBs in both NaCl and $CaCl_2$ conditions, and NOM-coated SLBs can partially or fully inhibit NP adsorption. It was also observed that nC_{60}NPs, but not AgNPs, had a specific interaction with NOM components, as indicated by the removal of NOM components from the SLB surface.

In marked contrast, NOM adsorption onto negatively charged SLBs was negligible in NaCl conditions and, as a result, subsequent NP adsorption onto the SLB surfaces was also minimal (Fig. 5A,B). In the presence of $CaCl_2$, there was some NOM adsorption, especially at the 10 ppm NOM concentration, down to an approximately -4 Hz shift (Fig. 5C,D). While the NOM coating did not promote AgNP adsorption onto the negatively charged SLBs, it did promote nC_{60}NP adsorption down to around -7 Hz under $CaCl_2$ conditions. These data further support that there is a particularly strong attraction between NOM components and nC_{60}NPs, and that attached NOM components under $CaCl_2$ conditions can promote nC_{60}NP adsorption while $CaCl_2$ conditions alone are insufficient to do so.

3.5. Effects of NOM-coated nanoparticles on nanoparticle adsorption

Fig. 6 presents the QCM-D measurement data for the adsorption of NOM-coated AgNP and nC_{60}NP adsorption onto positively charged SLBs, as outlined in Scenario 2. Prior to the experiment, AgNPs or nC_{60}NPs were mixed with NOM in the presence of 10 mM NaCl or $CaCl_2$ and subsequently added to the SLB platforms. In the NaCl condition, the adsorption of NOM-treated AgNPs led to a frequency shift of around -7 Hz and the magnitude was largely independent of the NOM concentration (Fig. 6A). By contrast, there was minimal adsorption of the NOM-treated nC_{60}NPs under the same condition (Fig. 6B). In the $CaCl_2$ condition, there was significantly greater adsorption of NOM-treated AgNPs and the magnitude of the frequency shift depended on the NOM concentration. The final frequency shift for NOM-treated

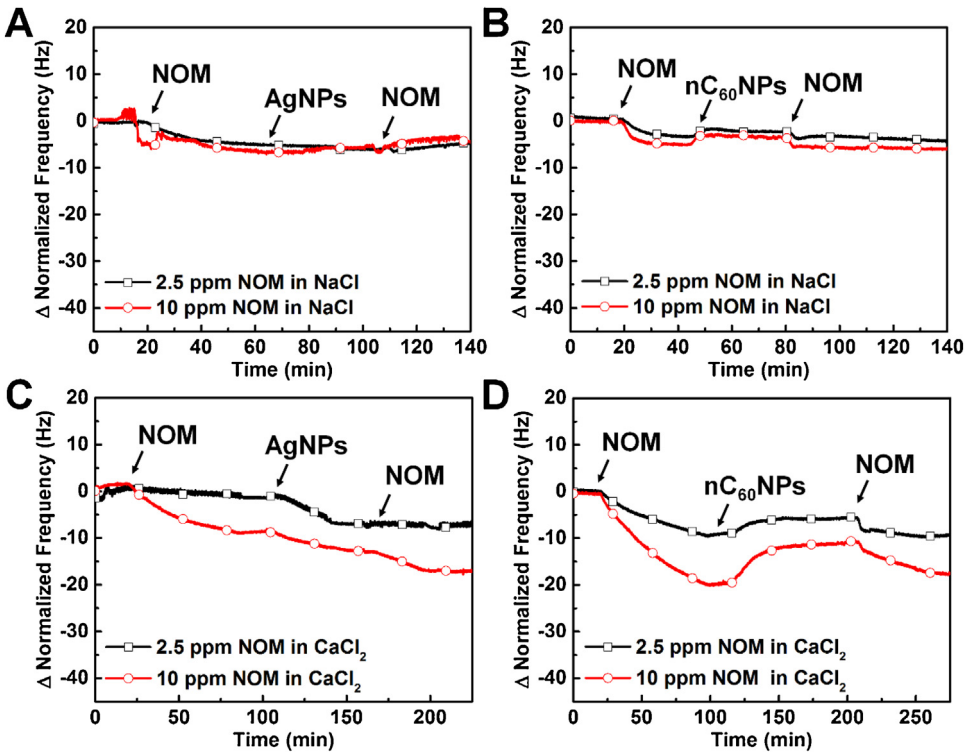

Fig. 4. Adsorption of AgNPs and nC_{60}NPs onto NOM-coated SLB platforms with positive membrane surface charge. QCM-D measurements track resonance frequency shifts. NOM was added to the SLB platform, then 2.5 ppm AgNPs or 450 nM nC_{60}NPs, and finally NOM again. Addition of (A) AgNPs or (B) nC_{60}NPs in 10 mM NaCl. Addition of (C) AgNPs or (D) nC_{60}NPs in 10 mM $CaCl_2$.

AgNP adsorption was around -17.9 ± 0.5 Hz and -39.1 ± 6.2 Hz at 2.5 ppm and 10 ppm NOM concentrations, respectively (Fig. 6C). Slight adsorption of the NOM-treated nC_{60}NPs was observed in the $CaCl_2$ condition, with minor frequency shits around -4 Hz (Fig. 6D). By contrast, NOM-treated AgNPs and nC_{60}NPs did not adsorb onto negatively charged SLBs (Fig. 7). Taken together, the findings sup-

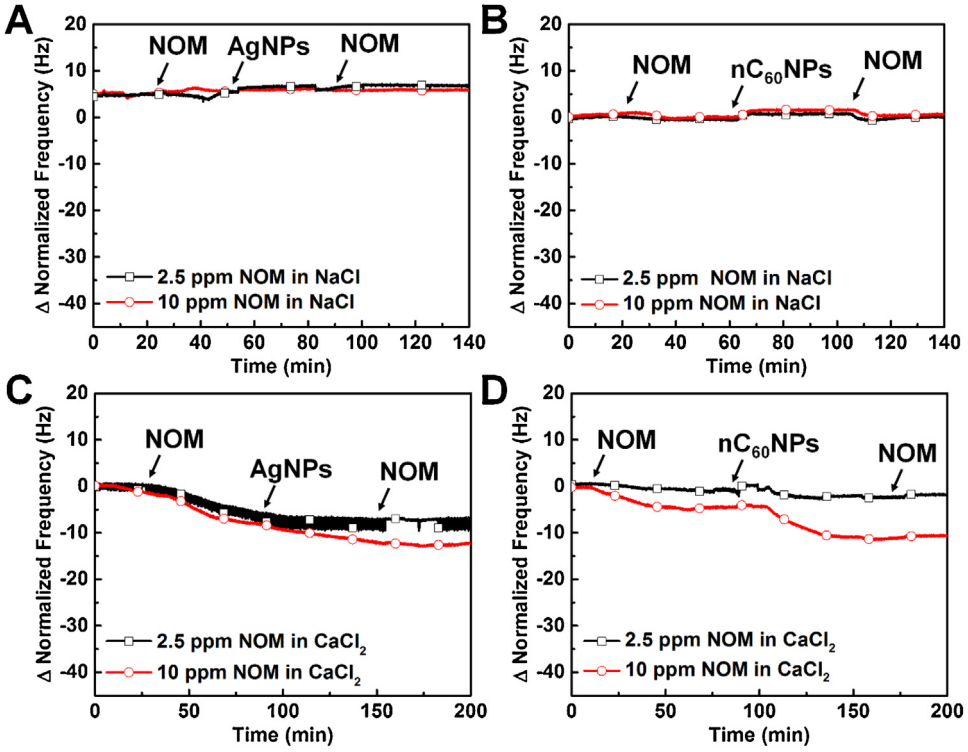

Fig. 5. Adsorption of AgNPs and nC_{60}NPs onto NOM-coated SLB platforms with negative membrane surface charge. QCM-D measurements track resonance frequency shifts. NOM was added to the SLB platform, then 2.5 ppm AgNPs or 450 nM nC_{60}NPs, and finally NOM again. Addition of (A) AgNPs or (B) nC_{60}NPs in 10 mM NaCl. Addition of (C) AgNPs or (D) nC_{60}NPs in 10 mM $CaCl_2$.

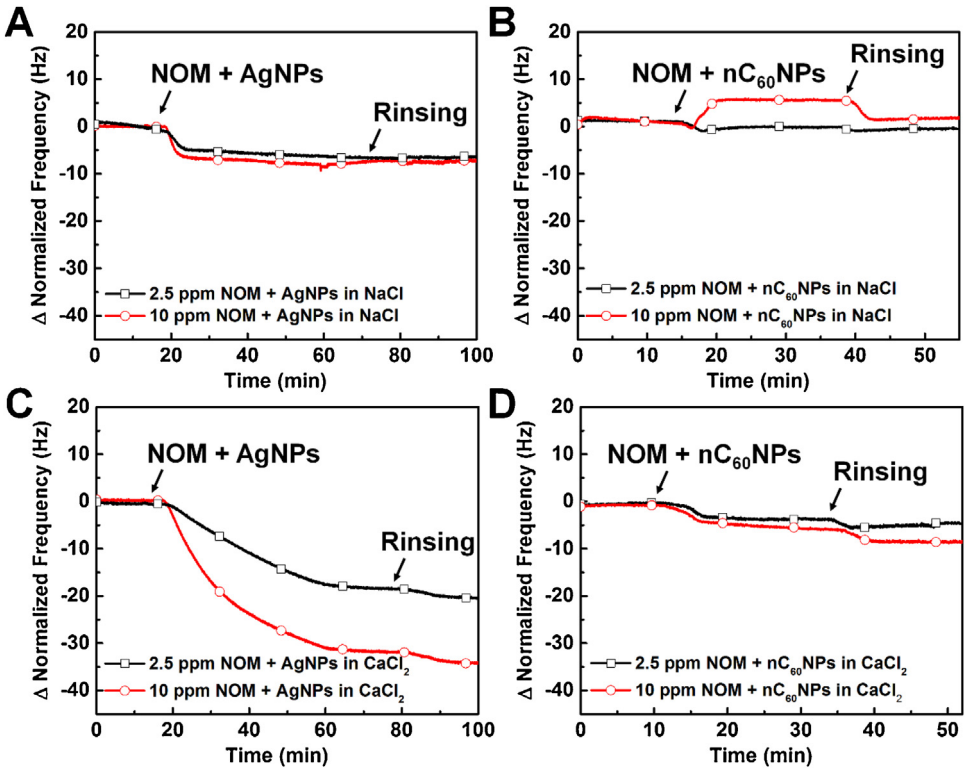

Fig. 6. Adsorption of NOM-coated AgNPs and nC_{60}NPs onto positively charged SLB platforms. QCM-D measurements track resonance frequency shifts. 2.5 or 10 ppm NOM + 2.5 ppm AgNPs or 450 nM nC_{60}NPs were added to the SLB platform. Addition of NOM-coated (A) AgNPs or (B) nC_{60}NPs in 10 mM NaCl. Addition of (C) AgNPs or (D) nC_{60}NPs in 10 mM $CaCl_2$.

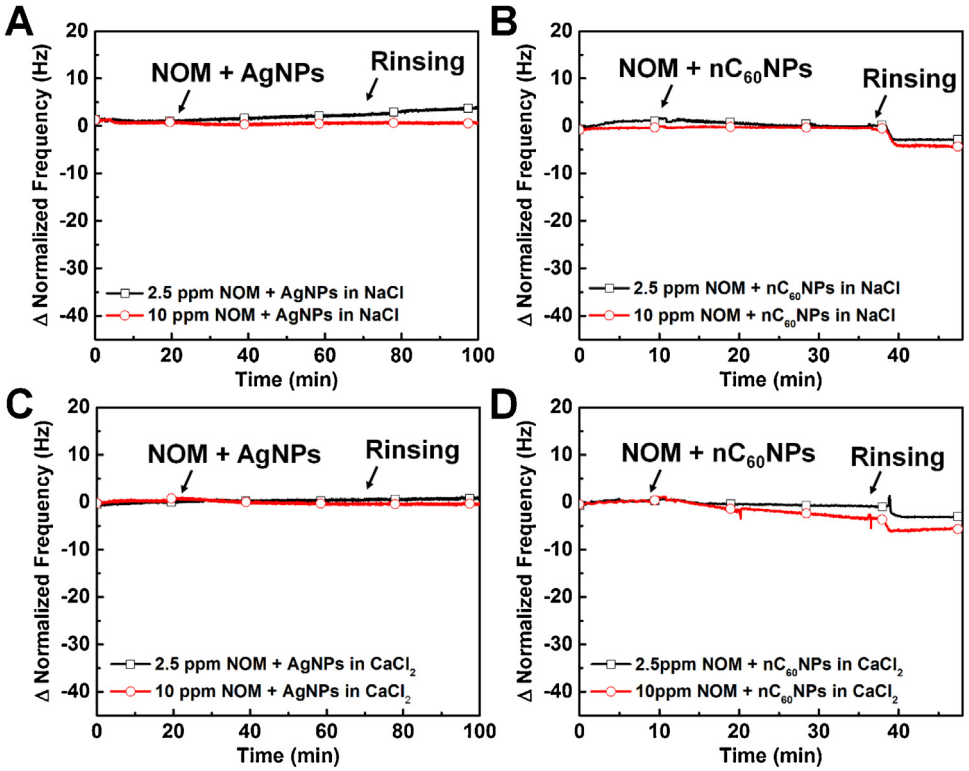

Fig. 7. Adsorption of NOM-coated AgNPs and nC_{60}NPs onto negatively charged SLB platforms. QCM-D measurements track resonance frequency shifts. 2.5 or 10 ppm NOM + 2.5 ppm AgNPs or 450 nM nC_{60}NPs were added to the SLB platform. Addition of NOM-coated (A) AgNPs or (B) nC_{60}NPs in 10 mM NaCl. Addition of (C) AgNPs or (D) nC_{60}NPs in 10 mM $CaCl_2$.

port that NOM has a minor effect on the interaction between AgNPs and positively charged SLBs, whereas NOM has a stronger influence on the interaction between nC_{60}NPs and positively charged SLBs. On the other hand, the interaction between the two types of NPs and negatively charged SLBs was negligible

While NOM has been shown to prevent iron and silver nanoparticles from adhering to cell membranes and hence limited toxicity in certain contexts, our findings provide a more complete mechanistic picture of how NOM can either promote or inhibit membrane-nanoparticle interactions depending on the membrane surface charge and electrolyte conditions [70,71]. Indeed, the influence of NOM on nanoparticle attachment was only previously studied under a limited set of monovalent salt conditions. As discovered herein, under certain conditions, NOM can increase nanoparticle adsorption onto lipid membranes and the specific effects depend on the type of nanoparticle and lipid membrane under consideration. Looking forward, there is exciting potential to further understand how NOM influences the biological activities of nanoparticles under different electrolyte conditions and to connect the physiochemical insights obtained herein with broader environmental consequences.

4. Conclusion

As presented herein, we investigated how membrane surface charge influences the adsorption of AgNPs and nC_{60}NPs onto SLB platforms under different electrolyte concentrations, and consequently how NOM influences these membrane-NP interactions. While the electrolyte conditions are simplified models of complex environmental systems, they offer insight into how monovalent and divalent cations influence NP adsorption onto charged lipid membranes. It was observed that bare, negatively charged AgNPs and nC_{60}NPs adsorb onto positively charged SLBs, whereas they do not adsorb onto negatively charged lipid bilayers—a finding consistent with attractive electrostatic forces mediating membrane association. For AgNPs, membrane adsorption onto positively charged SLBs was enhanced in the presence of divalent cations and NOM had differential effects on the membrane-AgNP interaction under these conditions. Pretreatment of SLBs with NOM partially inhibited subsequent AgNP adsorption, while NOM-coated AgNPs exhibited appreciably greater adsorption. On the other hand, the extent of nC_{60}NP adsorption onto positively charged SLBs was similar in the presence of monovalent or divalent cations. Strikingly, NOM treatment of SLBs or nC_{60}NPs almost fully inhibited membrane adsorption in monovalent conditions, as did NOM of nC_{60}NPs in divalent conditions. Overall, the data support that nC_{60}NPs have a particularly strong interaction with NOM components that can either impede adsorption (*via* NOM-NP interaction) or promote adsorption (*via* NOM-SLB interaction), whereas the effects of NOM on AgNP adsorption are relatively minor. It should be noted that the ionic strength conditions used in this study were relatively low, and charge shielding under higher ionic strength conditions would reduce the strength of electrostatic forces alone. Considering that NOM is inherently present in many important environmental systems, the experimental scenarios explored in this work provide insight into how NOM may influence membrane-nanoparticle interactions and suggest that these effects are linked to the affinity of NOM components to lipid membrane interfaces and the particular type of nanoparticle being considered.

Acknowledgments

This work was supported by the National Natural Science Foundation of China (Grant No. 21677097) and the National Science and Technology Major Projects of Water Pollution Control and Management of China (2014ZX07206001). The authors also wish to acknowledge support from the National Research Foundation of Singapore (NRF2015NRF-POC001-019) and Nanyang Technological University to N.J.C. M.S.C. was supported by the 2016 Hongik University Research Fund and the Ministry of Trade, Industry & Energy (MOTIE, Korea) under the Industrial Technology Innovation Program. No.10052106.

References

[1] M.L. Etheridge, S.A. Campbell, A.G. Erdman, C.L. Haynes, S.M. Wolf, J. McCullough, The big picture on nanomedicine: the state of investigational and approved nanomedicine products, Nanomed. Nanotechnol. Biol. Med. 9 (2013) 1–14.
[2] H. Wang, R. DeSousa, J. Gasa, K. Tasaki, G. Stucky, B. Jousselme, F. Wudl, Fabrication of new fullerene composite membranes and their application in proton exchange membrane fuel cells, J. Membr. Sci. 289 (2007) 277–283.
[3] T.M. Benn, P. Westerhoff, P. Herckes, Detection of fullerenes (C_{60} and C_{70}) in commercial cosmetics, Environ. Pollut. 159 (2011) 1334–1342.
[4] E. Fauss, The Silver Nanotechnology Commercial Inventory, University of Virginia, 2008.
[5] H.Y. Lee, H.K. Park, Y.M. Lee, S.B. Park, A practical procedure for producing silver nanocoated fabric and its antibacterial evaluation for biomedical applications, Chem. Commun. 28 (2007) 2959–2961.
[6] J. Fabrega, S.N. Luoma, C.R. Tyler, T.S. Galloway, J.R. Lead, Silver nanoparticles: behaviour and effects in the aquatic environment, Environ. Int. 37 (2011) 517–531.
[7] C. Levard, E.M. Hotze, G.V. Lowry, G.E. Brown Jr, Environmental transformations of silver nanoparticles: impact on stability and toxicity, Environ. Sci. Technol. 46 (2012) 6900–6914.
[8] R. Avanasi, W.A. Jackson, B. Sherwin, J.F. Mudge, T.A. Anderson, C60 fullerene soil sorption, biodegradation, and plant uptake, Environ. Sci. Technol. 48 (2014) 2792–2797.
[9] M. Farre, K. Gajda-Schrantz, L. Kantiani, D. Barcelo, Ecotoxicity and analysis of nanomaterials in the aquatic environment, Anal. Bioanal. Chem. 393 (2009) 81–95.
[10] D. Lin, X. Tian, F. Wu, B. Xing, Fate and transport of engineered nanomaterials in the environment, J. Environ. Qual. 39 (2010) 1896–1908.
[11] J.R. Peralta-Videa, L. Zhao, M.L. Lopez-Moreno, G. de la Rosa, J. Hong, J.L. Gardea-Torresdey, Nanomaterials and the environment: a review for the biennium 2008–2010, J. Hazard. Mater. 186 (2011) 1–15.
[12] J. McTeer, A.P. Dean, K.N. White, J.K. Pittman, Bioaccumulation of silver nanoparticles into Daphnia magna from a freshwater algal diet and the impact of phosphate availability, Nanotoxicity 8 (2013) 305–316.
[13] J.L. Luque-Garcia, R. Sanchez-Diaz, I. Lopez-Heras, P. Martin, C. Camara, Bioanalytical strategies for *in-vitro* and *in-vivo* evaluation of the toxicity induced by metallic nanoparticles, TrAC Trends Anal. Chem. 43 (2013) 254–268.
[14] C.M. Zhao, W.X. Wang, Biokinetic uptake and efflux of silver nanoparticles in *Daphnia magna*, Environ. Sci. Technol. 44 (2010) 7699–7704.
[15] M. Song, F. Wang, L. Zeng, J. Yin, H. Wang, G. Jiang, Co-exposure of carboxyl-functionalized single-walled carbon nanotubes and 17α-ethinylestradiol in cultured cells: effects on bioactivity and cytotoxicity, Environ. Sci. Technol. 48 (2014) 13978–13984.
[16] D.M. Mitrano, E.K. Lesher, A. Bednar, J. Monserud, C.P. Higgins, J.F. Ranville, Detecting nanoparticulate silver using single-particle inductively coupled plasma-mass spectrometry, Environ. Toxicol. Chem. 31 (2012) 115–121.
[17] M.L. Whitfield Aslund, H. McShane, M.J. Simpson, A.J. Simpson, J.K. Whalen, W.H. Hendershot, G.I. Sunahara, Earthworm sublethal responses to titanium dioxide nanomaterial in soil detected by ^{1}H NMR metabolomics, Environ. Sci. Technol. 46 (2011) 1111–1118.
[18] X.J. Tao, J.D. Fortner, B. Zhang, Y.L. He, Y.S. Chen, J.B. Hughes, Effect of aqueous stable fullerene nanocrystals (nC_{60}) on *Daphnia magna*: evaluation of sub-lethal reproductive responses and accumulation, Chemosphere 77 (2009) 1482–1487.
[19] K.L. Aillon, Y.M. Xie, N. El-Gendy, C.J. Berkland, M.L. Forrest, Effect of nanomaterial physicochemical properties on *in vivo* toxicity, Adv. Drug Deliv. Rev. 61 (2009) 457–466.
[20] E.P. Gray, J.G. Coleman, A.J. Bednar, A.J. Kennedy, J.F. Ranville, C.P. Higgins, Extraction and analysis of silver and gold nanoparticles from biological tissues using single particle inductively coupled plasma mass spectrometry, Environ. Sci. Technol. 47 (2013) 14315–14323.
[21] K.T. Kitchin, E. Grulke, B.L. Robinette, B.T. Castellon, Metabolomic effects in HepG2 cells exposed to four TiO_2 and two CeO_2 nanomaterials, Environ. Sci. Nano 1 (2014) 466–477.
[22] C. Gil-Allué, K. Schirmer, A. Tlili, M.O. Gessner, R. Behra, Silver nanoparticle effects on stream periphyton during short-term exposures, Environ. Sci. Technol. 49 (2015) 1165–1172.
[23] K.L. Chen, G.D. Bothun, Nanoparticles meet cell membranes: probing nonspecific interactions using model membranes, Environ. Sci. Technol. 8730880 (2014).

[24] S. Kang, M. Pinault, L.D. Pfefferle, M. Elimelech, Single-walled carbon nanotubes exhibiting strong antimicrobial activitity, Langmuir 23 (2007) 8670–8673.
[25] S.B. Liu, T.H. Zeng, M. Hofmann, E. Burcombe, J. Wei, R.R. Jiang, J. Kong, Y. Chen, Antibacterial activity of graphite, graphite oxide, graphene oxide, and reduced graphene oxide: membrane and oxidative stress, ACS Nano 3 (2011) 3891–3902.
[26] A. Lesniak, A. Salvati, M. Santos-Martinez, M.W. Radomski, K.A. Dawson, C. Aberg, Nanoparticle adhesion to the cell membrane and its effect on nanoparticle uptake efficiency, J. Am. Chem. Soc. 135 (2013) 1438–1444.
[27] M.R. de Planque, S. Aghdaei, T. Roose, H. Morgan, Electrophysiological characterization of membrane disruption by nanoparticles, ACS Nano 5 (2011) 3599–3606.
[28] R.P. Carney, Y. Astier, T.M. Carney, K. Voïtchovsky, P.H. Jacob Silva, F. Stellacci, Electrical method to quantify nanoparticle interaction with lipid bilayers, ACS Nano 7 (2013) 932–942.
[29] G.J. Gordillo, Z. Krpetic, M. Brust, Interactions of gold nanoparticles with a phospholipid monolayer membrane on mercury, ACS Nano 8 (2014) 6074–6080.
[30] B. Wang, L. Zhang, S.C. Bae, S. Granick, Nanoparticle-induced surface reconstruction of phospholipid membranes, Proc. Natl. Acad. Sci. U. S. A. 105 (2008) 18171–18175.
[31] R.V. Goreham, V.C. Thompson, Y. Samura, C.T. Gibson, J.G. Shapter, I. Köper, Interaction of silver nanoparticles with tethered bilayer lipid membranes, Langmuir 31 (2015) 5868–5874.
[32] J.A. Jackman, W. Knoll, N.-J. Cho, Biotechnology applications of tethered lipid bilayer membranes, Materials 5 (2012) 2637–2657.
[33] C. Merz, W. Knoll, M. Textor, E. Reimhult, Formation of supported bacterial lipid membrane mimics, Biointerphases 3 (2008) FA41–FA50.
[34] M. Hyldgaard, D.S. Sutherland, M. Sundh, T. Mygind, R.L. Meyer, Antimicrobial mechanism of monocaprylate, Appl. Environ. Microbiol. 78 (2012) 2957–2965.
[35] S.R. Tabaei, J.-H. Choi, G. Haw Zan, V.P. Zhdanov, N.-J. Cho, Solvent-assisted lipid bilayer formation on silicon dioxide and gold, Langmuir 30 (2014) 10363–10373.
[36] S.R. Tabaei, J.A. Jackman, S.-O. Kim, V.P. Zhdanov, N.-J. Cho, Solvent-assisted lipid self-assembly at hydrophilic surfaces: factors influencing the formation of supported membranes, Langmuir 31 (2015) 3125–3134.
[37] A. Mashaghi, S. Mashaghi, I. Reviakine, R.M. Heeren, V. Sandoghdar, M. Bonn, Label-free characterization of biomembranes: from structure to dynamics, Chem. Soc. Rev. 43 (2014) 887–900.
[38] X.T. Liu, K.L. Chen, Interactions of graphene oxide with model cell membranes: probing nanoparticle attachment and lipid bilayer disruption, Langmuir 31 (2015) 12076–12086.
[39] Y. Roiter, M. Ornatska, A.R. Rammohan, J. Balakrishnan, D.R. Heine, S. Minko, Interaction of nanoparticles with lipid membrane, Nano Lett. 8 (2008) 941–944.
[40] P. Yi, K.L. Chen, Interaction of multiwalled carbon nanotubes with supported lipid bilayers and vesicles as model biological membranes, Environ. Sci. Technol. 47 (2013) 5711–5719.
[41] G.V. Lowry, K.B. Gregory, S.C. Apte, J.R. Lead, Transformations of nanomaterials in the environment, Environ. Sci. Technol. 46 (2012) 6893–6899.
[42] Y. Zhang, Y. Chen, P. Westerhoff, J. Crittenden, Impact of natural organic matter and divalent cations on the stability of aqueous nanoparticles, Water Res. 43 (2009) 4249–4257.
[43] M. Baalousha, Y. Nur, I. Römer, M. Tejamaya, J. Lead, Effect of monovalent and divalent cations: anions and fulvic acid on aggregation of citrate-coated silver nanoparticles, Sci. Total Environ. 454 (2013) 119–131.
[44] B.J.R. Thio, M.O. Montes, M.A. Mahmoud, D.W. Lee, D.X. Zhou, A.A. Keller, Mobility of capped silver nanoparticles under environmentally relevant conditions, Environ. Sci. Technol. 46 (2011) 6985–6991.
[45] J.T.K. Quik, I. Lynch, K.V. Hoecke, C.J.H. Miermans, K.A.C.D. Schamphelaere, C.R. Janssen, K.A. Dawson, M.A.C. Stuart, D.V.D. Meent, Effect of natural organic matter on cerium dioxide nanoparticles settling in model fresh water, Chemosphere 81 (2010) 711–715.
[46] A.A. Keller, H. Wang, D. Zhou, H.S. Lenihan, G. Cherr, B.J. Cardinale, R. Miller, Z. Ji, Stability and aggregation of metal oxide nanoparticles in natural aqueous matrices, Environ. Sci. Technol. 44 (2010) 1962–1967.
[47] C. Levard, E.M. Hotze, G.V. Lowry, G.E. Brown Jr., Environmental transformations of silver nanoparticles: impact on stability and toxicity, Environ. Sci. Technol. 46 (2012) 6900–6914.
[48] R.S. Summers, P.V. Roberts, Activated carbon adsorption of humic substances: i. Heterodisperse mixtures and desorption, J. Colloid Interface Sci. 122 (1988) 367–381.
[49] R.S. Summers, P.V. Roberts, Activated carbon adsorption of humic substances: II. Size exclusion and electrostatic interactions, J. Colloid Interface Sci. 122 (1988) 382–397.
[50] J. Buffle, K.J. Wilkinson, S. Stoll, M. Filella, J. Zhang, A generalized description of aquatic colloidal interactions: the three-colloidal component approach, Environ. Sci. Technol. 32 (1998) 2887–2899.
[51] N. Yousefi, N. Tufenkji, Probing the interaction between nanoparticles and lipid membranes by quartz crystal microbalance with dissipation monitoring, Front. Chem. 4 (2016) 1–8.
[52] N. Yousefi, A. Wargenau, N. Tufenkji, Toward more free-floating model cell membranes: method development and application to their interaction with nanoparticles, ACS Appl. Mater. Interfaces 8 (2016) 14339–14348.
[53] M. Tejamaya, I. Römer, R.C. Merrifield, J.R. Lead, Stability of citrate, PVP, and PEG coated silver nanoparticles in ecotoxicology media, Environ. Sci. Technol. 46 (2012) 7011–7017.
[54] L.K. Duncan, J.R. Jinschek, P.J. Vikesland, C_{60} colloid formation in aqueous systems: effects of preparation method on size, structure, and surface charge, Environ. Sci. Technol. 42 (2007) 173–178.
[55] M.-H. Jang, S. Lee, Y.S. Hwang, Characterization of silver nanoparticles under environmentally relevant conditions using asymmetrical flow field-flow fractionation (AF4), PLoS One 10 (2015) e0143149.
[56] K.L. Chen, M. Elimelech, Influence of humic acid on the aggregation kinetics of fullerene (C_{60}) nanoparticles in monovalent and divalent electrolyte solutions, J. Colloid Interface Sci. 309 (2007) 126–134.
[57] K.A. Huynh, K.L. Chen, Aggregation kinetics of citrate and polyvinylpyrrolidone coated silver nanoparticles in monovalent and divalent electrolyte solutions, Environ. Sci. Technol. 45 (2011) 5564–5571.
[58] M. Terashima, S. Nagao, Solubilization of [60] fullerene in water by aquatic humic substances, Chem. Lett. 36 (2007) 302–303.
[59] B. Xie, Z.H. Xu, W.H. Guo, Q.L. Li, Impact of natural organic matter on physicochemical properties of aqueous C_{60} nanoparticles, Environ. Sci. Technol. 42 (2008) 2853–2859.
[60] O. Furman, S. Usenko, B.L.T. Lau, Relative importance of the humic and fulvic fractions of natural organic matter in the aggregation and deposition of silver nanoparticles, Environ. Sci. Technol. 47 (2013) 1349–1356.
[61] X. Li, J.J. Lenhart, Aggregation and dissolution of silver nanoparticles in natural surface water, Environ. Sci. Technol. 46 (2012) 5378–5386.
[62] H. Mashayekhi, S. Ghosh, P. Du, B.S. Xing, Effect of natural organic matter on aggregation behavior of C_{60} fullerene in water, J. Colloid Interface Sci. 374 (2012) 111–117.
[63] M. Delay, T. Dolt, A. Woellhaf, R. Sembritzki, F.H. Frimmel, Interactions and stability of silver nanoparticles in the aqueous phase: influence of natural organic matter (NOM) and ionic strength, J. Chromatogr. A 1218 (2011) 4206–4212.
[64] H. Hyung, J.-H. Kim, Natural organic matter (NOM) adsorption to multi-walled carbon nanotubes: effect of NOM characteristics and water quality parameters, Environ. Sci. Technol. 42 (2008) 4416–4421.
[65] S.R. Tabaei, J.A. Jackman, M.C. Kim, S. Yorulmaz, S. Vafaei, N.-J. Cho, Biomembrane fabrication by the solvent-assisted lipid bilayer (SALB) method, J. Visual. Exp. 106 (2015).
[66] S.R. Tabaei, S. Vafaei, N.-J. Cho, Fabrication of charged membranes by the solvent-assisted lipid bilayer (SALB) formation method on SiO_2 and Al_2O_3, Phys. Chem. Chem. Phys. 17 (2015) 11546–11552.
[67] S. Yorulmaz, J.A. Jackman, W. Hunziker, N.-J. Cho, Influence of membrane surface charge on adsorption of complement proteins onto supported lipid bilayers, Colloids Surf. B: Biointerfaces 148 (2016) 270–277.
[68] T.A. Spurlin, A.A. Gewirth, Effect of C_{60} on solid supported lipid bilayers, Nano Lett. 7 (2007) 531–535.
[69] Z. Wang, S. Yang, Effects of fullerenes on phospholipid membranes: a Langmuir monolayer study, ChemPhysChem 10 (2009) 2284–2289.
[70] Z. Li, K. Greden, P.J.J. Alvarez, K.B. Gregory, G.V. Lowry, Adsorbed polymer and NOM limits adhesion and toxicity of nano scale zerovalent iron to *E. coli*, Environ. Sci. Technol. 44 (2010) 3462–3467.
[71] S.M. Wirth, G.V. Lowry, R.D. Tilton, Natural organic matter alters biofilm tolerance to silver nanoparticles and dissolved silver, Environ. Sci. Technol. 46 (2012) 12687–12696.